

# Increase of critical currents and peak effect in Mo substituted $\text{YBa}_2\text{Cu}_3\text{O}_7$

K. Rogacki

*Institute of Low Temperature and Structure Research,  
Polish Academy of Sciences, 50-950 Wrocław, P.O.Box 1410, Poland and  
Laboratory for Solid State Physics, ETH Zürich, 8093 Zürich, Switzerland*

B. Dabrowski and O. Chmaissem

*Physics Department, Northern Illinois University, DeKalb, IL 60115*

(Dated: July 17, 2021)

Superconducting critical currents  $j_c > 10^5$  A/cm<sup>2</sup> at temperatures  $T \sim 50$  K and magnetic fields  $B \sim 6$  T are reported for the  $\text{YBa}_2\text{Cu}_{3-x}\text{Mo}_x\text{O}_{7+d}$  compound with  $x = 0.02$ . Clear evidence for the increased pinning force  $F_p$  was found from a peak effect present for  $j_c(B)$ . The pinning force was analyzed by a scaling procedure using Kramer's approach. For a wide range of fields and temperatures, we were able to express all  $F_p$  data as a single function of a reduced field  $b = B/B_k$ , where the scaling field  $B_k \ll H_{c2}$  was related to the irreversibility field  $B_{irr}$ . Analyses of the field dependence of  $j_c(B, T)$  and  $F_p(b)$  show that the effective pinning centers act as weakly interacting extended point-like defects. We propose that the pinning centers are randomly distributed small defects, most likely the dimers of  $\text{MoO}_6$  octahedra in the  $\text{CuO}$  chains.

PACS numbers: 74.25.Sv, 74.72.Bk, 74.62.Bf, 74.62.Dh

## I. INTRODUCTION

One of the most promising areas where high temperature superconductors (HTSC) can find immediate utilization is large-scale power application. Such applications require development of materials capable of sustaining critical currents on the order of  $j_c > 10^5$  A/cm<sup>2</sup> at liquid nitrogen temperatures and displaying only a weak dependence on applied magnetic fields. These critical current requirements are difficult to satisfy in ceramic HTSC materials. However, increased  $j_c$  values and weaker  $j_c$  dependencies on applied field can be achieved by increasing the flux pinning, which depends on the interaction of magnetic vortices with crystal defects, and with second-phase impurities including magnetic nanoparticles.<sup>1,2,3,4,5,6,7,8</sup> One of the most effective methods of increasing the flux pinning at intermediate range of applied fields is creation of columnar irradiation defects.<sup>9,10,11</sup> Another effective method is introduction of microscopic grains of the  $\text{Y}_2\text{BaCuO}_5$  phase that are the most efficient at the intermediate range of temperatures.<sup>2,4</sup> Both these methods are rather difficult to implement in large-scale applications. Thus, simpler methods are required for intensifying flux pinning in the range of increased temperatures and high magnetic fields. We show here that optimized chemical substitution could be one such methods for the  $\text{YBa}_2\text{Cu}_3\text{O}_7$  type superconductors.

In  $\text{YBa}_2\text{Cu}_3\text{O}_7$  (Y123) several cation substitutions were made for the small ion (copper) and for the large ions (barium and yttrium).<sup>12,13,14</sup> In most cases, substitutions for copper were found to rapidly decrease  $T_c$ . For the Fe and Al substitutions on the Cu-chain site,  $T_c$  remained constant up to 5 and 10 %, respectively.<sup>13</sup> For Ga,  $T_c$  decreased more rapidly resulting in the complete absence of superconductivity at 10 % doping.<sup>15</sup> A modest

increase of  $T_c$  was conceivably observed by substitution of 2-5 % Co.<sup>13</sup> For Sr substituted  $\text{YBa}_{2-y}\text{Sr}_y\text{Cu}_3\text{O}_7$ , a gradual decrease of  $T_c$  was observed up to the solubility limit found around  $y = 1$  under normal synthesis conditions.<sup>14</sup> Interestingly, when the high oxygen pressure anneal (HPA) was applied for the Mo-substituted  $\text{YBaSrCu}_{3-x}\text{Mo}_x\text{O}_{7+d}$  compound,  $T_c$  increased from 81 to 87 K.<sup>3</sup> However, decrease of  $T_c$  and  $j_c$  has been reported for the Mo-substituted Y123 compounds synthesized under ambient pressure.<sup>16</sup> Here we show that both the higher  $T_c$  and increased  $j_c$  can be achieved for the  $\text{YBa}_2\text{Cu}_{3-x}\text{Mo}_x\text{O}_{7+d}$  system if appropriate synthesis and oxygenation conditions are applied.

In this work, an increase of the superconducting  $T_c$ , intragrain persistent critical current density  $j_c$ , and irreversibility field  $B_{irr}$ , was achieved for the  $\text{YBa}_2\text{Cu}_{3-x}\text{Mo}_x\text{O}_{7+d}$  compound by determining the optimum composition, synthesis, and annealing conditions. The structural and superconducting properties of the optimized materials with  $T_c \approx 90$ -93 K are examined and compared with recently published data for similar compounds. The magnetization  $M(B)$  isotherms are measured over wide field and temperature ranges to derive  $j_c(B)$  and  $j_c(T)$  which reveal a pronounced peak effect. A scaling approach is used to determine the mechanism responsible for the peak effect. We show that substitution of Mo results in creation of additional pinning centers and formation of the significant peak effect at elevated fields and temperatures. We propose that the small-size defects in the  $\text{CuO}$  chains, most likely the  $\text{Mo}_2\text{O}_{11}$  dimers made of nearest neighbor  $\text{MoO}_6$  octahedra, may act as effective pinning centers similar to that seen in  $\text{YBaSrCu}_{3-x}\text{Mo}_x\text{O}_{7+d}$  compounds.<sup>3</sup> The  $\text{Mo}_2\text{O}_{11}$  dimers may locally perturb superconductivity in the  $\text{CuO}_2$  planes by providing additional weakly interacting pinning centers which increase the total pinning force.

Finally, we show an important difference between the pinning mechanisms observed for the pure Y123 ( $x = 0$ ) and the Mo-substituted ( $0 < x \leq 0.05$ ) samples for which substitution results in the pronounced maximum in  $j_c(B)$  at high fields.

Recently, intriguing clustering of Al ions substituted for Cu in the Cu-O chains of  $\text{YBa}_2\text{Cu}_3\text{O}_7$  has been reported.<sup>17</sup> This clustering, studied by positron annihilation and x-ray diffraction experiments, induces the localization of hole carriers, weakens the function of the Cu-O chains as carrier reservoir, and as a consequence, suppresses superconductivity. If the Al clusters are separated one from another by at least few unit cells, they should disturb superconductivity only locally. A similar effect of small  $\text{Mo}_2\text{O}_{11}$  defects in the Cu-O chains separated by several unit cells is considered in this work as a possible mechanism responsible for creation of pinning centers in the Mo substituted  $\text{YBa}_2\text{Cu}_3\text{O}_7$  samples.

## II. EXPERIMENTAL DETAILS

Polycrystalline samples of  $\text{YBa}_2\text{Cu}_{3-x}\text{Mo}_x\text{O}_{7+d}$  with  $0 \leq x \leq 0.2$  were synthesized from a mixture of Y, Mo, and Cu oxides, and Ba carbonate. These samples compose a subset of a wider range of recently investigated materials  $\text{YBa}_{2-y}\text{Sr}_y\text{Cu}_{3-x}\text{Mo}_x\text{O}_{7+d}$  shown in Fig. 1. Samples were fired in air and oxygen at 880-920 °C for several days with frequent intermediate grindings. Normal pressure anneals (NPA) were done in pure oxygen for 12 h at 600 °C followed by slow cooling to room temperature. High pressure anneals (HPA) were done in pure oxygen using 250-300 bar at 650 °C followed by slow cooling to room temperature. Sample homogeneity was checked by powder x-ray diffraction on a Rigaku D/MAX Diffractometer using  $\text{CuK}\alpha$  radiation. Structural parameters and oxygen contents were refined from time-of-flight neutron powder diffraction data collected on the General Purpose Powder Diffractometer (GPPD) at the Argonne National Laboratory Intense Pulsed Neutron Source (IPNS). Diffraction data for the NPA and HPA samples were collected at room temperature. High-resolution backscattering data were analyzed using the Rietveld method with the General Structure Analysis System (GSAS) code.<sup>18</sup> In the analysis, background, absorption, peak width, and extinction parameters were refined, together with the lattice parameters, atomic positions, and isotropic temperature factors for the cations and oxygen atoms. The oxygen contents were also determined by thermogravimetric analysis using a Cahn TG171 system with slow (0.6 deg/min) heating and cooling rates. The sizes and shapes of the grains were examined using a Hitachi Scanning Electron Microscope (SEM).

Resistivity,  $R$ , ac susceptibility,  $\chi$ , and dc magnetization,  $M$ , were measured with a Quantum Design Physical Properties Measurement System (PPMS) equipped with 7 T superconducting magnet. For resistivity mea-

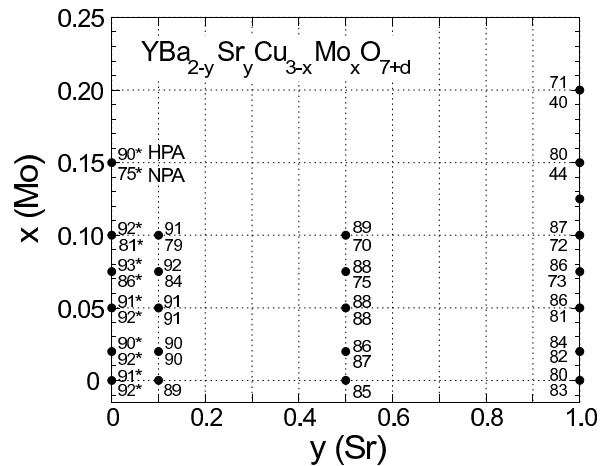


FIG. 1: Superconducting transition temperatures,  $T_c$ , for the  $\text{YBa}_{2-y}\text{Sr}_y\text{Cu}_{3-x}\text{Mo}_x\text{O}_{7+d}$  samples annealed in oxygen at normal pressure (NPA, lower numbers) and high pressure (HPA, upper numbers). Stars mark  $T_c$ 's for samples investigated in this work.

surements, solid pieces of the sintered samples were used and the standard four-lead dc method was applied with a current density of about 0.2 A/cm<sup>2</sup>. Solid pieces were also used for  $\chi$  measurements to estimate the superconducting shielding effect. Powder samples with masses of about 200 mg were employed for both  $\chi$  and  $M$  measurements to obtain the superconducting volume fraction, critical currents, and irreversibility fields (Figures 3 to 11). The susceptibility was taken upon warming from the zero-field-cooled (ZFC) state using the ac field of 1 Oe at 200 Hz. For these measurements, the real  $\chi'$  and imaginary  $\chi''$  parts of the signal were collected. As will be discussed in following sections,  $\chi''$  was used to determine the irreversibility field  $B_{irr}$ . This is based on a principle that when the energy losses are of hysteretic type, the energy absorption  $\chi''$  is proportional to the area of the magnetization hysteresis loop which is non-zero in the presence of irreversibility of  $M(T)$ .

## III. SYNTHESIS AND INITIAL CHARACTERIZATION

The optimum synthesis and annealing conditions of temperature and oxygen pressure were determined to maximize the superconducting transition temperature  $T_c$ . Samples were fired several times in air, 1 % oxygen in Ar, and pure oxygen at increasing temperatures, checked for phase purity, annealed under several oxygen pressure and temperatures, and checked for  $T_c$ . All compositions were single phase when synthesized in air or oxygen at 880-920 °C. Small amounts of impurities ( $\approx 3$  %) were present for synthesis temperatures both lower than 880 °C, due to incomplete reaction, and higher than 920 °C, due to partial melting. High-pressure oxygen anneals at 250-300 bar and at temperatures around

650 °C followed by slow cooling (0.2 deg/min) were found to be optimal to increase the oxygen content and to attain the highest  $T_c$  for samples obtained from synthesis in pure oxygen. After the same HPA, the  $T_c$ 's of the samples synthesized in air and 1 % oxygen were consistently lower by several degrees. Attempts to synthesize the  $\text{YBa}_2\text{Cu}_{3-x}\text{Mo}_x\text{O}_{7+d}$  compounds directly at high oxygen pressure of 600 bar at 950 °C produced multiphase materials with  $T_c$ 's  $\sim 60$  K.

Figure 1 shows the maximum  $T_c$ 's we have obtained for the  $\text{YBa}_{2-y}\text{Sr}_y\text{Cu}_{3-x}\text{Mo}_x\text{O}_{7+d}$  samples with  $0 \leq x \leq 0.2$  and  $0 \leq y \leq 1$ . The upper and lower numbers denote the  $T_c$ 's obtained after anneal in oxygen and high pressure, respectively. The oxygen index,  $d$ , is clearly positive for the Mo-substituted compositions (e.g., for the  $y = 1$  samples,  $d = 0.16$  and  $0.3$  for  $x = 0.1$  and  $0.2$ , respectively).<sup>3</sup> The  $T_c$  for the NPA  $y = 0$  samples decreases rapidly with  $x$  from 92 K for  $x = 0$  to 81 K for  $\text{YBa}_2\text{Cu}_{2.9}\text{Mo}_{0.1}\text{O}_{7.14}$ . However, the HPA restores  $T_c \approx 92$  K for all  $0 < x \leq 0.1$  samples. The main effect of the HPA is to fill the oxygen vacancies in the  $\text{CuO}$  chains (i.e., to increase the hole-carrier concentration) and to introduce the inter-chain oxygen atoms (i.e., to form defects). These electronic and structural changes cause important modifications of the superconducting properties that will be discussed in subsequent sections.

Figure 2 shows normalized resistance for three  $\text{YBa}_2\text{Cu}_{3-x}\text{Mo}_x\text{O}_{7+d}$  samples with  $x = 0.02$ ,  $0.05$ , and  $0.075$ , after NPA and HPA. Clearly,  $T_c$  depends on both the Mo substitution level  $x$  and the oxygen content. The NPA samples show rapid decrease of  $T_c$  with  $x$  (see also Fig. 1) resulting in a transition temperature of 86 K for  $x = 0.075$ . The samples with  $x = 0$ ,  $0.02$ , and  $0.05$  behave as optimally doped or slightly over-doped; their  $T_c$  decreases after the HPA process, which increases the oxygen content and thus, most likely, enhances the charge-carrier concentration. The samples with  $x > 0.05$  show under-doped properties; after the HPA process, their  $T_c$  increases. Similar features are also observed for the  $\text{YBa}_{2-y}\text{Sr}_y\text{Cu}_{3-x}\text{Mo}_x\text{O}_{7+d}$  samples with the Sr-substitution level  $y = 0.1$ ,  $0.5$ , and  $1$  (see Fig. 1). The normal-state resistivity of  $\text{YBa}_2\text{Cu}_{3-x}\text{Mo}_x\text{O}_{7+d}$  displays a non-linear temperature dependence that changes with both  $x$  and  $d$ . This behavior, as well as complex dependence of the superconducting transition width, cannot be easily interpreted for polycrystalline materials; we investigate these effects by studying the transport properties of the recently synthesized single crystals.

The shapes and sizes of the grains were determined by SEM. Most of the grains have a plate-like shape, are well connected, and have a size distribution ranging from 5 to 20  $\mu\text{m}$ , with an average main plate dimension of about 10 and 8  $\mu\text{m}$  for the samples with  $x \leq 0.02$  and  $x \geq 0.05$ , respectively. Thus, to estimate the effective superconducting volume fraction of the grains and to evaluate the density of the intragrain persistent critical currents, an average grain size of 10 and 8  $\mu\text{m}$  was taken for the samples with  $x \leq 0.02$  and  $x \geq 0.05$ , respectively.

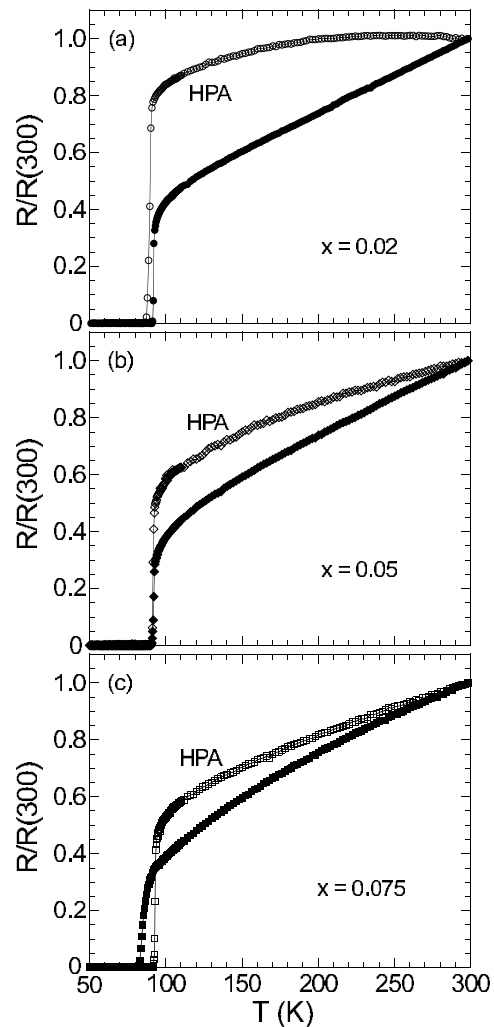


FIG. 2: Normalized resistance,  $R/R(300)$ , versus temperature for the  $\text{YBa}_2\text{Cu}_{3-x}\text{Mo}_x\text{O}_{7+d}$  samples with  $x = 0.02$  (a),  $0.05$  (b), and  $0.075$  (c), after annealing in oxygen at normal pressure (closed symbols) and high pressure (open symbols, HPA). As a result of HPA, the superconducting  $T_c$  remains constant, decreases or increases, depending on the substitution level.

Adopting the main plate dimension as a characteristic scaling length for the randomly oriented grains results in a certain underestimation of the intragrain critical currents calculated from the Bean model. Note, that for the  $\text{YBaSrCu}_3\text{O}_{7+d}$  compound, studied previously, the grains were smaller (3-4  $\mu\text{m}$ ) and more round revealing a systematic decrease of the grain size with Sr-substitution in the Y123 compound.<sup>3</sup>

#### IV. CRYSTAL STRUCTURE

Neutron powder diffraction experiments were carried out to determine the exact structural details of our Mo-substituted YBCO materials. Initial refinements were

performed assuming the structural and atomic positions of the parent YBCO material. Attempts to refine the site occupancies of the two independent copper sites [chain (Cu1) and planar (Cu2) sites] resulted in the planar Cu2 sites being completely occupied only by Cu while the occupancy of the Cu1 chain sites was significantly reduced because of the Mo substitution on this site. However, determining of the exact Cu and Mo site occupancies was not possible because of the low contrast between their neutron scattering lengths (7.718 fm and 6.715 fm for Cu and Mo, respectively). As such, in all subsequent refinements we fixed the Cu and Mo contents at their nominal values. On the other hand, refinements of the oxygen site occupancies demonstrated that all sites are essentially full within one or two standard deviation except for the oxygen site (O1) that is located in the blocking layer between the Cu1 chain atoms. Additionally, a significantly larger than expected temperature factor was refined for this oxygen atom indicating that atoms occupying this site must be shifted off their special positions ( $0 \frac{1}{2} 0$ ). Subsequent refinements demonstrated that O1 oxygen atoms actually occupy atomic positions ( $x \frac{1}{2} 0$ ) that are slightly shifted off the a-axis and that their site occupancy decreases with increasing Mo content. A second oxygen atom (O5) was introduced at ( $\frac{1}{2} y 0$ ) and found to have a site occupancy that increases with increasing Mo content. As such, the total oxygen content in this layer would be the sum of both the site occupancies of O1 and O5. A summary of all significant structural parameters is listed in Table I.

The careful examination of the structural results leads to several important conclusions: 1- the orthorhombicity factor ( $\epsilon = b-a$ ) of the samples decreases significantly as the Mo content increases. Notice that the a-axis increases while the b-axis decreases as a function of increasing Mo content. 2- the site occupancy of O1 decreases significantly from 0.87 for  $x = 0.05$  to 0.66 for  $x = 0.15$  for the as-made samples and that the high-pressure annealing either leaves the occupancy of this site unchanged or reduces its content. 3- the site occupancy of O5 increases significantly from 0.17 to 0.43 and 0.54 for the NPA  $x = 0.05$ , 0.1 and 0.15 samples, respectively. High-pressure annealing results in increasing the oxygen content of this site contrary to what is observed for the O1 site. 4- for the NPA samples, the overall oxygen content increases up to 7.20 atom per formula unit with increasing Mo content. 5- the high-pressure annealing forces extra oxygen atoms into the structure with the oxygen content increasing from 7.04 to 7.07, 7.14 to 7.23, and 7.20 to 7.27 for the  $x = 0.05$ , 0.1 and 0.15 samples, respectively. Here we note that the Mo-substituted samples prepared under normal oxygen pressures possess oxygen contents that are significantly greater than the oxygen content of the unsubstituted YBCO parent material ( $\simeq 6.97$ ) (see the total oxygen contents near the bottom of Table I). Thus, the difference in oxygen content between the substituted and unsubstituted materials may be directly attributed to the presence of Mo atoms in the host structure. As

	Position	Parameter	x = 0.05	x = 0.05	x = 0.1	x = 0.1	x = 0.15	x = 0.15
			NPA	HPA	NPA	HPA	NPA	HPA
a (Å)			3.8387(2)	3.8397(2)	3.8562(2)	3.8593(2)	3.8662(2)	3.8670(1)
b (Å)			3.8817(2)	3.8800(2)	3.8736(3)	3.8704(2)	3.8714(2)	3.8709(1)
c (Å)			11.7069(6)	11.6944(7)	11.7143(8)	11.6998(7)	11.7228(6)	11.7072(4)
Vol. (Å <sup>3</sup> )			174.44(3)	174.22(3)	174.98(3)	174.76(3)	175.46(3)	175.24(2)
c/a ratio			3.049704	3.045655	3.037783	3.031586	3.032125	3.027463
c/b ratio			3.015921	3.014021	3.024138	3.022892	3.028052	3.024413
$\epsilon = b-a$			0.0430	0.0403	0.0174	0.0111	0.0052	0.0039
Y	(1/2 1/2 1/2)	Uiso (Å <sup>2</sup> )	0.69(3)	0.71(4)	0.84(3)	0.77(4)	0.77(3)	0.84(3)
Ba	(1/2 1/2 z)	z	0.1852(1)	0.1843(2)	0.1856(1)	0.1844(2)	0.1864(1)	0.1852(1)
		Uiso (Å <sup>2</sup> )	0.96(3)	1.01(4)	1.25(4)	1.36(5)	1.06(4)	1.09(3)
Cu1	(0 0 0)	Uiso (Å <sup>2</sup> )	0.76(3)	0.80(4)	1.00(4)	0.97(4)	0.92(3)	0.90(3)
Cu2	(0 0 z)	z	0.35572(7)	0.3553(1)	0.35621(9)	0.3557(1)	0.35725(7)	0.35660(7)
		Uiso (Å <sup>2</sup> )	0.64(2)	0.65(3)	0.83(3)	0.87(3)	0.70(2)	0.67(2)
O1	(x 1/2 0)	x	0.040(1)	0.040(2)	0.045(2)	0.046(3)	0.044(4)	0.038(3)
		Uiso (Å <sup>2</sup> )	1.2(1) [2.0]	1.3(1) [2.1]	1.3(2) [2.3]	1.5(3) [2.8]	1.8(4) [3.1]	0.5(2) [1.5]
		n	0.87(1)	0.88(1)	0.71(2)	0.73(3)	0.66(3)	0.58(2)
O2	(1/2 0 z)	z	0.3787(1)	0.3785(2)	0.3785(3)	0.3778(4)	0.3813(3)	0.3755(3)
		Uiso (Å <sup>2</sup> )	0.89(4)	0.81(6)	0.86(8)	1.0(1)	1.2(1)	0.88(9)
O3	(0 1/2 z)	z	0.3786(1)	0.3786(2)	0.3779(3)	0.3780(4)	0.3763(3)	0.3817(3)
		Uiso (Å <sup>2</sup> )	0.75(5)	0.83(6)	0.90(8)	0.7(1)	0.43(8)	0.67(8)
O4	(0 0 z)	z	0.1587(1)	0.1590(1)	0.1588(1)	0.1596(2)	0.1587(1)	0.1593(1)
		Uiso (Å <sup>2</sup> )	1.04(4)	1.05(5)	1.39(5)	1.31(6)	1.35(4)	1.33(4)
O5	(1/2 y 0)	y	0.044(5)	0.033(9)	0.035 (7)	0.042(5)	0.054(4)	0.061(4)
		Uiso (Å <sup>2</sup> )	0.7(4) [1.4]	1.1(5) [1.4]	3.2(5) [3.5]	2.3(5) [2.8]	1.8(5) [2.7]	3.3(4) [4.6]
		n	0.17(1)	0.19(1)	0.43(2)	0.50(3)	0.54(4)	0.69(3)
Total Oxygen (7-d)			7.04	7.07	7.14	7.23	7.20	7.27
R <sub>p</sub> (%)			3.73 [3.91]	4.35 [4.46]	3.88 [3.99]	4.94 [5.07]	3.71 [3.98]	3.79 [4.03]
R <sub>wp</sub> (%)			5.18 [5.37]	6.12 [6.23]	5.48 [5.60]	6.89 [7.04]	5.34 [5.60]	5.28 [5.55]
$\chi^2$			2.056 [2.203]	1.753 [1.815]	2.039 [2.125]	2.426 [2.532]	1.492 [1.639]	1.628 [1.799]

TABLE I: Refined structural parameters for YBa<sub>2</sub>Cu<sub>3-x</sub>Mo<sub>x</sub>O<sub>7+d</sub> samples annealed in oxygen at normal pressure (NPA) and high pressure (HPA). Values in square parentheses are obtained from refinements with O1 and O5 occupying special positions ( $0 \frac{1}{2} 0$ ) and ( $\frac{1}{2} 0 0$ ), respectively.

such, the  $x = 0.05$ , 0.1 and 0.15 samples exhibit additional 0.07(2), 0.17(2) and 0.23(2) oxygen atoms, respectively (assuming an oxygen content of 6.97 for the parent YBCO material). We can easily note that the ratio between the extra oxygen atoms and Mo content is nearly 3:2 for all the samples, which means that three additional oxygen atoms are introduced into the structure for every pair of Mo atoms. This ratio can be explained by the presence of Mo pairs pointing preferentially in the direction of the a-axis in a fashion similar to that observed for YBaSrCu<sub>3-x</sub>Mo<sub>x</sub>O<sub>7+d</sub> and YSr<sub>2</sub>Cu<sub>3-x</sub>Mo<sub>x</sub>O<sub>7+d</sub> ( $M = \text{Mo, W}$ ).<sup>3,19</sup> We note that the other ordering schemes are also possible to preserve the 2:3 ratio of the added Mo and oxygen atoms, respectively. For example, four MoO<sub>6</sub> octahedra replacing a square of four Cu atoms in the chain layers would give the same ratio. Larger clusters are also possible with the same ratio. However, as the sizes of clusters grow, we would need to consider

them as inclusions of an impurity phase,  $\text{MoBa}_2\text{YCu}_2\text{O}_8$ , which we do not observe in our diffraction measurements. Thus, the  $\text{Mo}_2\text{O}_{11}$  and possibly the limited amount of  $\text{Mo}_4\text{O}_{20}$  clusters seem to be the most likely defects explaining consistently our results. The clusters such as dimers or squares of  $\text{MoO}_6$  octahedra in the  $\text{CuO}$  chains disturb locally the crystallographic structure and the oxidation state of the  $\text{Cu}$  atoms, and interfere with the charge transfer between the chains and planes, and thus perturb locally the superconducting state. These effects, which may result in creation of pinning centers, are discussed in the following chapter.

## V. MAGNETIC CHARACTERIZATION AND CRITICAL CURRENTS

### A. Superconducting Volume Fraction

The shielding effect and the effective superconducting volume fraction of grains were estimated from the ac susceptibility measurements performed at 5 K. The average density of the solid samples was measured to be  $5.1 (\pm 0.1) \text{ g/cm}^3$ ; i.e. about 80 % of the theoretical material density ( $6.3 \text{ g/cm}^3$ ). The absolute  $\chi'$  values for solid samples were obtained using the measured sample volume and correcting the data by taking into account demagnetizing effects. For our solid samples, for all compositions, the corrected  $\chi'$  values are about 5 % lower than the ideal value,  $-1/4\pi$ , which would indicate perfect shielding. The effective superconducting volume fraction of the grains can be, in principle, estimated for both solid and powder samples when the grains are decoupled in magnetic fields large enough to depress superconductivity in the intergrain region. For our solid samples, it was not possible to separate grains even at quite high fields and temperatures. Thus, powder samples were used for evaluation of the superconducting volume fraction, critical currents, and the irreversibility field. For powder samples, almost complete grain separation is observed for a field of 1 T at all temperatures down to 5 K. Taking into consideration the grain demagnetizing factor ( $N \approx 0.33$ ), the effective superconducting volume fraction of grains is estimated to be between 35 and 65 %, depending on the substitution level. This confirms bulk superconductivity and, moreover, attests to good quality of our samples when compared with Y123 material ( $\sim 70 \%$ ).<sup>20,21</sup>

### B. Critical Current Density

Magnetization hysteresis loops,  $M(B)$ , were measured at constant temperatures for powder samples to determine the intragrain persistent critical current density,  $j_c$ . Several examples of the  $M(B)$  curves are shown in Fig. 3 and Fig. 4 for  $T = 5$  and 50 K, respectively. By comparing the shapes and sizes of these hysteresis loops, it becomes immediately clear that the  $j_c(B)$  properties change

significantly with the temperature and degree of Mo substitution. Such behavior is expected when the dominant pinning mechanism varies between different types, as discussed in Ref. 22. The irreversibility of the magnetization, which is proportional to the persistent critical current density, is the largest for the  $x = 0.02$  sample. In addition, a pronounced widening of the magnetization loop, the fishtail effect, is observed for that sample at 50 K (see Fig. 4). The high oxygen pressure anneal reduces the irreversibility of the  $M(B)$  loops, however, it simultaneously shifts the maximum of the fishtail effect to much higher fields. This suggests that HPA creates new types of pinning centers that are effective at higher vortex densities, but also suppresses those which are present for samples with smaller oxygen content. At 5 K (see Fig. 3), no fishtail effect is observed for any sample. This may be explained by the fact that at low temperatures the superconducting coherence length,  $\xi$ , is comparable to the distance between the  $\text{CuO}_2$  double planes,  $\sim 8.5 \text{ \AA}$ , and the region between the double planes acts as the dominant intrinsic pinning center for every sample studied. The reduction of the  $M(B)$  loops by HPA for  $x = 0$  and 0.02 may be caused in part by a small decrease in  $T_c$  (see Fig. 2). The  $x = 0.05$  sample displays a noticeable increase of the  $M(B)$  loops after HPA which does not change  $T_c$ . One reason for this increase may be additional oxygen, introduced into the chains region, which can act as another weak, point-like pinning centers. This is supported by structural results obtained from neutron powder diffraction and by thermogravimetric measurements which show that the HPA increases the oxygen content from  $d = 0.04$  to 0.07. The  $M(B)$  results show that the optimal Mo substitution level for the largest  $j_c$  is around  $x = 0.02$ .

The extended Bean critical-state model was applied to calculate the persistent critical current density from magnetization measurements by using the relation  $j_c(\text{A/cm}^2) = k\Delta M/w$ , where  $\Delta M$  is the width of the  $M(B)$  loop in  $\text{emu/cm}^3$ ,  $w$  is a scaling length in cm, and  $k$  is a shape coefficient.<sup>23</sup> For our randomly oriented plate-like grains,  $k = 30$  was taken judiciously. The  $\Delta M(B)$  values at fields above the first magnetization peak were used to make the extended Bean model applicable.<sup>24</sup> These fields are close to or above the full penetration field, so they approximately satisfy the condition of the parallel orientation of the external field. Consequently, the component of  $j_c$  parallel to the external field seems to be negligible compared to the component perpendicular to the field, and thus, it is possible to accurately determine the value of  $j_c$ . The smallest values of  $\Delta M$  which could be reliably separated from the noise of the magnetometer were approximately  $1 \cdot 10^{-4}$  and  $0.5 \cdot 10^{-4} \text{ emu/g}$  (corresponding to the critical current densities of about 20 and  $10 \text{ A/cm}^2$ ) for the pure and substituted samples, respectively. The grain diameter was taken as the size of the current loops,  $w$ , for dc applied fields high enough to separate grains. This was deduced from the ac susceptibility measurements performed at various dc fields. The sepa-

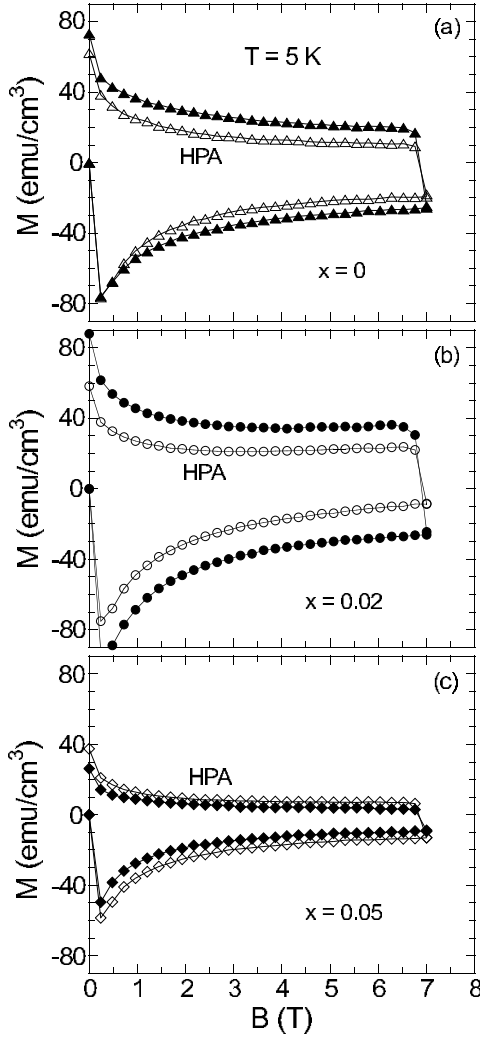


FIG. 3: Magnetization half-loops measured at 5 K for the  $\text{YBa}_2\text{Cu}_{3-x}\text{Mo}_x\text{O}_{7+d}$  samples with  $x = 0$  (a), 0.02 (b), and 0.05 (c) annealed in oxygen at normal pressure (closed symbols) and high pressure (open symbols, HPA).

ration of grains was confirmed by the absence of a second maximum in  $\chi''(T)$  that would mark the transition to the superconducting state for the intergrain material. The grain decoupling field was about 1 T at temperatures of about 60, 55 and 50 K for the powder samples with  $x = 0$ , 0.05 and 0.1, respectively. However, for fields above 1 T, the intergrain coupling was estimated to be small even at 5 K. Thus, we conclude that for fields above 1 T, the intergrain component of  $j_c$  can be neglected at all relevant temperatures and the average grain diameter can be taken as the scaling length.

Figure 5 shows  $j_c$  as a function of magnetic field at temperatures of 5, 35, and 50 K for the  $\text{YBa}_2\text{Cu}_{3-x}\text{Mo}_x\text{O}_{7+d}$  samples with  $x = 0$ , 0.02, 0.05, and 0.075 prepared at NPA and HPA conditions. At 5 K, the nearly field-independent  $j_c$  is the largest for  $x = 0.02$  at about  $2 \cdot 10^6 \text{ A/cm}^2$ . At this temperature, the difference between the  $x = 0$  and 0.02 samples is relatively small, most

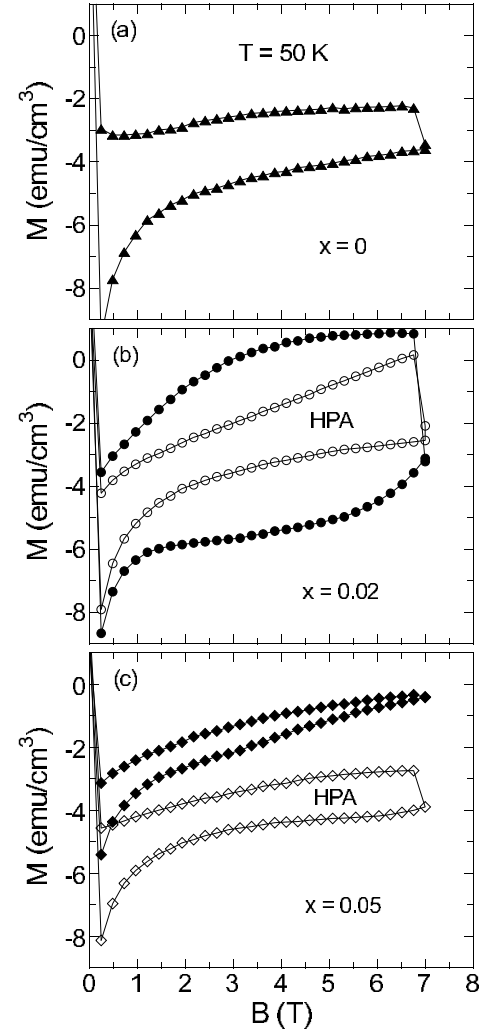


FIG. 4: Magnetization half-loops measured at 50 K for the  $\text{YBa}_2\text{Cu}_{3-x}\text{Mo}_x\text{O}_{7+d}$  samples with  $x = 0$  (a), 0.02 (b), and 0.05 (c) annealed in oxygen at normal pressure (closed symbols) and high pressure (open symbols, HPA). A large fishtail effect appears for the Mo-substituted sample with  $x = 0.02$ .

likely because the coherence length,  $\xi$ , is similar to the width of the pinning region between the superconducting  $\text{CuO}_2$  double planes. The influence of the Mo substitution is clearly observed at elevated temperatures, where the  $x = 0.02$  sample shows a huge increase of  $j_c$  over the  $x = 0$  sample. While enhancement as large as 30 to 50 % is observed at low temperatures, the substitution-created peak effect (PE) leads to 100 and 250 % increase of  $j_c$  at 35 and 50 K, respectively. Figure 6 shows  $j_c(B)$  at 77 K for the  $x = 0$ , 0.02, and 0.05 samples prepared at NPA and HPA conditions. In a field of 1.5 T,  $j_c(1.5 \text{ T}) \simeq 2 \cdot 10^3 \text{ A/cm}^2$  for the non-substituted sample and increases to about  $1 \cdot 10^4 \text{ A/cm}^2$  for the substituted sample with  $x = 0.02$ . At higher fields,  $j_c$  falls below  $100 \text{ A/cm}^2$  at 5 and 6 T for the  $x = 0$  and 0.02 samples, respectively. The HPA process affects  $j_c$  in two ways. For the pure and slightly substituted samples, HPA barely

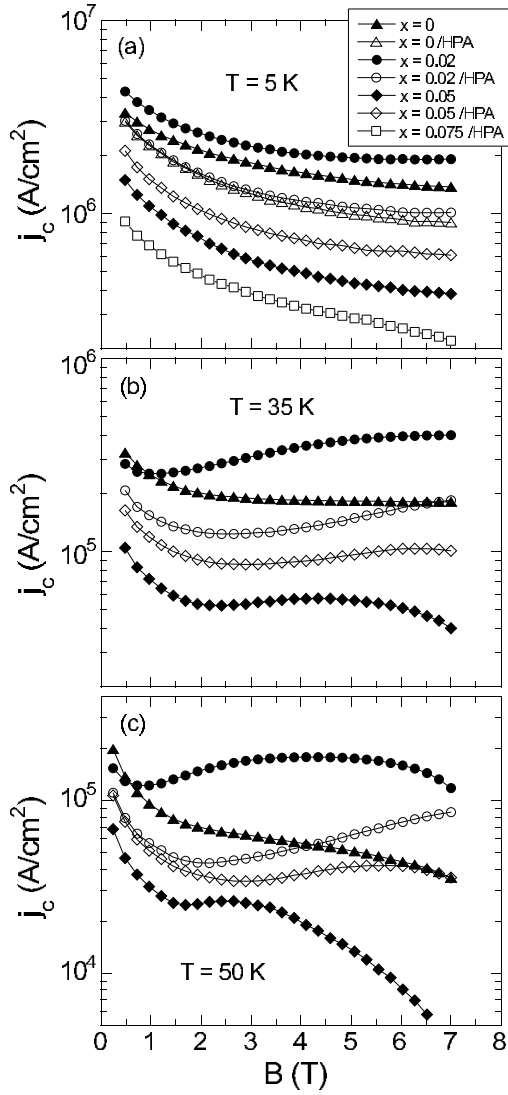


FIG. 5: Persistent critical currents,  $j_c$ , versus magnetic field at 5, 35, and 50 K for the  $\text{YBa}_2\text{Cu}_{3-x}\text{Mo}_x\text{O}_{7+d}$  samples with  $x = 0$  (triangles), 0.02 (circles), 0.05 (diamonds), and 0.075 (squares) annealed in oxygen at normal pressure (closed symbols) and high pressure (open symbols, HPA). An extended peak effect (fishtail for magnetization loops) is observed for the substituted compounds only.

reduces  $T_c$  while strongly suppressing  $j_c$ . This is most likely because by introducing a small amount of excess oxygen into the chain region, the HPA produces disordered point-like defects that reduce the superconducting volume fraction of the material. However, at moderate temperatures, HPA shifts PE to higher fields (see Fig. 5) probably as a result of weakly interacting pinning centers originated from these point-like defects. For samples with a higher substitution level ( $0.05 \leq x \leq 0.075$ ), the HPA increases  $j_c$  in the wide temperature range from 5 to 70 K. This increase can be qualitatively explained as a result of charge doping that increases  $T_c$  for  $x \geq 0.05$ . At temperatures close to  $T_c$ , HPA decreases  $j_c$  for all substi-

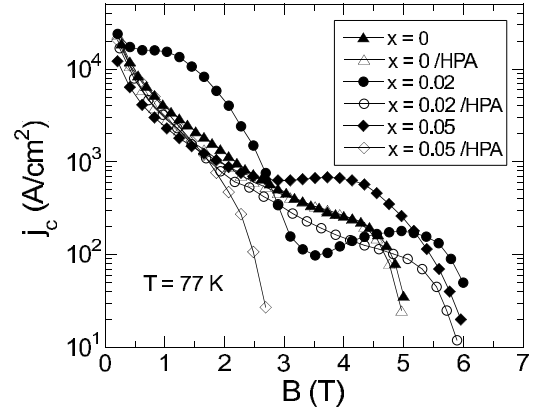


FIG. 6: Persistent critical currents,  $j_c$ , versus magnetic field at 77 K for the  $\text{YBa}_2\text{Cu}_{3-x}\text{Mo}_x\text{O}_{7+d}$  samples with  $x = 0$  (triangles), 0.02 (circles), and 0.05 (diamonds) annealed in oxygen at normal pressure (closed symbols) and high pressure (open symbols, HPA).

tuted samples, most likely due to the point-like defects that can reduce the irreversibility field,  $B_{irr}$ .<sup>25</sup> A significant reduction of  $B_{irr}$  by HPA has been observed for our substituted samples; this effect will be discussed in the next section.

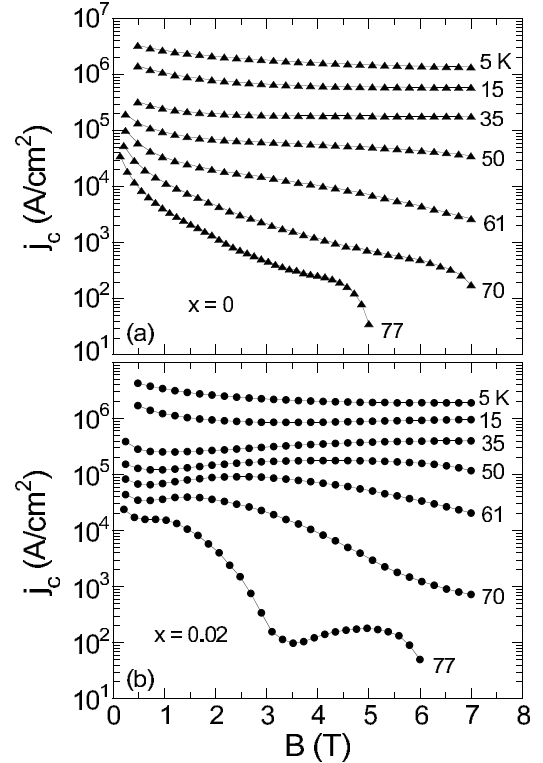


FIG. 7: Persistent critical currents,  $j_c$ , as a function of magnetic field at several temperatures from 5 to 77 K for the  $\text{YBa}_2\text{Cu}_{3-x}\text{Mo}_x\text{O}_{7+d}$  samples with  $x = 0$  (a) and 0.02 (b) annealed in oxygen at normal pressure.

Comparison of critical current properties at several

temperatures between 5 and 77 K is shown in Fig. 7 for NPA samples of  $\text{YBa}_2\text{Cu}_{3-x}\text{Mo}_x\text{O}_{7+d}$  with  $x = 0$  and 0.02. There are three regions of  $j_c$  dependence on  $B$  for  $x = 0$ . At low fields,  $j_c$  has a weaker than exponential decrease for all temperatures, similar to other high temperature superconductors. At higher fields below 35 K, a roughly exponential dependence is observed, extending to at least 7 T. At higher temperatures, the range of exponential dependence narrows and is followed by a more rapid decrease, especially above 70 K. Thus, PE is not observed for the  $x = 0$  sample. Figure 7(b) shows that for  $x = 0.02$  the region of the exponential decrease of  $j_c(B)$  exists only at temperatures below 15 K. At higher temperatures, a large maximum appears, shifting to lower fields with increasing temperature. This PE is a result of the fishtail effect seen for the magnetization loops (Fig. 4). For temperatures above 65 K, the second maximum of  $j_c(B)$  develops at high fields. The increase of  $j_c$  for  $x = 0.02$  seems to be more remarkable at 70 K, where the second maximum develops at fields higher than 7 T. At low fields and in the single-vortex pinning regime, a simple summation of the individual microscopic pinning forces leads to the relation  $j_c \sim B^\alpha$ , where  $\alpha = -1/2$ .<sup>26,27</sup> For our samples with  $x = 0, 0.05$ , and 0.075, this relation can be observed at fields  $B < 1.5$  T in the temperature range from 5 to 65 K. However, for the samples with  $x = 0.05$  and 0.075,  $j_c \sim B^\alpha$  with  $\alpha = -1/2$  is always observed over a narrower magnetic field range when compared with the sample with  $x = 0$ . For the optimally substituted compound with  $x = 0.02$ , no such dependence of  $j_c(B)$  is observed. These results suggest that collective rather than single-vortex pinning is present at moderate fields for the Mo-substituted samples. At higher fields, the characteristic  $j_c(B) \sim B^\alpha$  dependence has not been observed over any extended range of field or temperature making the analysis of the pinning mechanism more difficult and less useful.

Figures 5 through 7 show that the significant effect of the Mo-substitution on the pinning properties of Y123 is present at elevated temperatures and fields where a large PE in  $j_c(B)$  is observed. At elevated temperatures, point-like defects such as individual Mo-ions in the CuO chains are not capable of effective pinning because the interaction potential is smeared out by the thermal oscillation of vortices.<sup>25,28</sup> Thus, we suggest that the PE observed in our Mo-substituted samples at temperatures above 30 K is the result of more extended defects. This is consistent with our neutron diffraction results and oxygen-content measurements which provide evidence for existence of such extended defects in the form of the  $\text{Mo}_2\text{O}_{11}$  dimers (and possibly also  $\text{Mo}_4\text{O}_{20}$  clusters) formed from nearest neighbor  $\text{MoO}_6$  octahedra. This conclusion is in agreement with results reported for the melt textured Nd123 compound, where the pronounced PE was observed and interpreted as a result of weakly-interacting, small clusters of point-like defects.<sup>25</sup>

Superior pinning properties of the  $x = 0.02$  sample are more obvious when  $j_c$  is plotted as a function of tem-

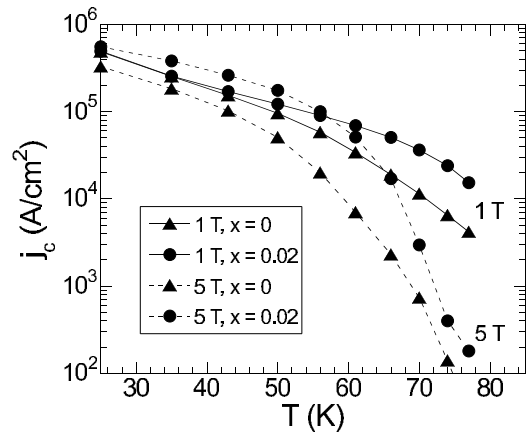


FIG. 8: Temperature dependence of persistent critical currents,  $j_c$ , for the  $\text{YBa}_2\text{Cu}_{3-x}\text{Mo}_x\text{O}_{7+d}$  samples with  $x = 0$  (triangles) and 0.02 (circles) annealed in oxygen at normal pressure. The  $j_c(T)$  dependencies are shown at the fields of 1 T (solid line) and 5 T (broken line).

perature. Figure 8 shows  $j_c(T)$  for the  $x = 0$  and 0.02 samples at fields of 1 and 5 T. The  $j_c(T)$  shows negative curvature for both  $x = 0$  and 0.02 from 30 to 70 K in high fields. However at 1 T, whereas  $j_c(T)$  for the  $x = 0$  sample shows the same negative curvature,  $j_c(T)$  for the  $x = 0.02$  sample shows positive curvature below 50 K. The resulting increase of  $j_c(T)$  at 1 T over the values obtained for the  $x = 0$  sample can be well modeled for temperatures between 50 and 80 K by an exponential expression  $j_c(T) = j_c(0)\exp[-3(T/T^*)^2]$  with two fitting parameters:  $j_c(0) = 4.3 \cdot 10^5$  A/cm<sup>2</sup> and  $T^* = 0.85T_c$ . This expression was proposed to account for pinning by correlated disorder<sup>29,30</sup> and was observed for  $\text{Bi}_2\text{Sr}_2\text{CaCu}_2\text{O}_8$  single crystals with columnar defects generated by heavy ion irradiation.<sup>31</sup> This similarity suggests that the observed increase of  $j_c$  for Mo-substituted samples could be caused by pinning centers that are partially ordered along the  $c$ -axis. An important point to note is that at 1 T the  $j_c(T) \gtrsim 10^4$  A/cm<sup>2</sup> shows a maximal enhancement at about 72-76 K, i.e., at temperatures close to the liquid nitrogen temperature. These values of  $j_c$ , observed for the  $x = 0.02$  polycrystalline sample, are similar to, or higher than, those obtained for the textured Y123/Y211 composites.<sup>2</sup> Because in polycrystalline samples  $j_c$  is determined by the current component perpendicular to the  $ab$ -plane, even higher critical currents are expected for the Mo-substituted textured materials when  $j_c$  flows in the  $ab$ -plane only.

### C. Irreversibility line and pinning analysis

The irreversibility field,  $B_{irr}$ , was derived from the ac susceptibility measured as a function of temperature at constant applied dc fields. Each "irreversibility point" ( $B_{irr}, T_{irr}$ ) of the irreversibility line  $B_{irr}(T)$  was obtained by determining a characteristic tempera-



ture,  $T_{irr}$ , at which the imaginary part of the ac susceptibility,  $\chi''$ , begins to differ from zero. Below this temperature, both the critical current density and the ac losses differ from zero; i.e., the magnetization is irreversible. Thus,  $T_{irr}$  denotes a temperature below which resistivity is zero and a diamagnetic signal appears for the real part of the ac susceptibility,  $\chi'$ .<sup>23</sup> Because the sensitivity of our ac susceptibility measurements is at least 100 times higher than that of our dc magnetization measurements ( $2 \cdot 10^{-5}$  emu), the  $B_{irr}(T)$  curves obtained from ac susceptibility are taken as the upper limits of the  $B_{irr}(T)$  lines derived from magnetization.<sup>3</sup>

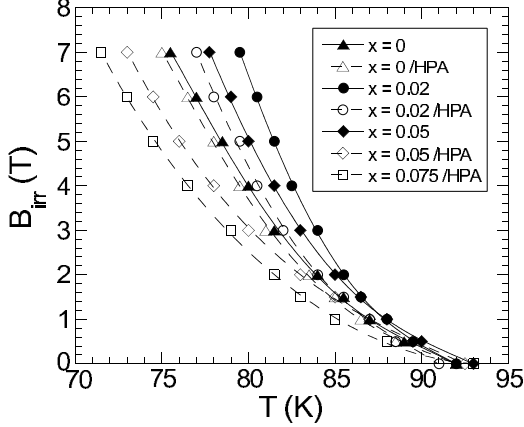


FIG. 9: Temperature dependence of the irreversibility field,  $B_{irr}$ , obtained from ac susceptibility measurements for the  $\text{YBa}_2\text{Cu}_{3-x}\text{Mo}_x\text{O}_{7+d}$  samples with  $x = 0$  (triangles), 0.02 (circles), 0.05 (diamonds), and 0.075 (squares) annealed in oxygen at normal pressure (closed symbols) and high pressure (open symbols, HPA). The lines are guides for the eye only.

The irreversibility lines determined by ac susceptibility are shown in Fig. 9 for the NPA and HPA powder samples. The highest irreversibility line and the largest slope of  $dB_{irr}/dT$  were obtained for the NPA sample with  $x = 0.02$ . Increasing the Mo-substitution shifts the  $B_{irr}(T)$  line to lower fields. However, even for the  $x = 0.05$  sample, the line is still above that of the  $x = 0$  sample. A large decrease of  $B_{irr}(T)$  is observed for all Mo-substituted samples after HPA. This decrease may be caused by introduction of uncorrelated defects (additional oxygen ions) and is consistent with results obtained for  $j_c(B)$  closer to  $T_c$  (see Fig. 6) where a sudden drop of  $j_c$  below 10 A/cm<sup>2</sup> appears at fields that correspond to  $B_{irr}$ . A small difference between  $B_{irr}$  and fields where the drop appears is caused by different sensitivity in measurements used to obtain  $B_{irr}$  (ac susceptibility) and  $j_c$  (dc magnetization). The temperature dependence of  $B_{irr}(T)$  can be expressed by a power-law relation  $B_{irr} \sim (1 - T/T_c)^n$ , with  $n \simeq 1.7$  and 1.6 derived for the  $x = 0$  and 0.02 samples, respectively. For  $x = 0$ , the power relation with  $n = 1.7$  fits very well over the whole temperature range shown from 75 K to  $T_c = 92$  K. For  $x = 0.02$ , the power law holds only over much narrower temperature range from about 83 K to  $T_c$ . A

small difference of the exponent near  $T_c$  points to rather minor changes of the electronic structure introduced by the Mo substitution. Strongly divergent behavior of the  $B_{irr}(T)$  at lower temperatures for the  $x = 0.02$  sample results from increased volume pinning force.

From the above-analyzed behavior of  $j_c$ ,  $B_{irr}$ , and  $T_c$ , it appears that the Mo-substitution mainly changes the pinning properties of the Y123 material. The substitution introduces pinning centers that are most likely  $\text{Mo}_2\text{O}_{11}$  dimers located in the CuO chains, as concluded from the neutron results. The dimers may act as pinning centers because they induce extended distortions in the structure and, therefore, may locally perturb superconductivity in the  $\text{CuO}_2$  planes. The individual perturbation with a dimension of 2-3 unit cells in the  $ab$ -plane is comparable to the superconducting coherence length,  $\xi$ , and therefore may act as an effective pinning center. It is plausible that the dimers order partially along the  $c$ -axis to form a number of oriented "columnar" defects.<sup>32,33</sup> To analyze the relevant pinning mechanism related to the pinning centers introduced by the Mo-substitution, we turn now to discussion of the volume pinning force as a function of field by using the scaling procedure.

The volume pinning force is defined by a formula  $F_p(B) = j_c \cdot B$ , where  $F_p$  is in N/m<sup>3</sup>,  $j_c$  in A/m<sup>2</sup>, and  $B$  in T (i.e., the main features of the  $F_p(B)$  are similar to  $j_c(B)$  as shown in Figs. 5-7). Two maximums in  $j_c(B)$  and  $F_p(B)$  are observed at 77 K for the NPA sample with  $x = 0.02$  (see Fig. 6). The first maximum appears at low fields ( $B \simeq 1.2$  T) and the second at higher fields ( $\simeq 5$  T) close to a critical field where a sudden drop of the pinning force is observed. Such behavior of  $F_p(B)$  is generally consistent with the prediction of the static collective pinning theory for the pinning centers of average force;<sup>34</sup> for example, small clusters of dislocations like the  $\text{Mo}_2\text{O}_{11}$  dimers. For the sample with a larger Mo-substitution level ( $x = 0.05$ , see Fig. 6), the low-field maximum disappears while the high-field maximum increases above that observed for the  $x = 0.02$  sample. According to the static collective pinning theory, this behavior indicates that the pinning arises from weakly interacting centers as a function of increased concentration. This is in fact the case for our highly substituted samples, where an introduction of additional  $\text{Mo}_2\text{O}_{11}$  dimers results in a denser and therefore smoother pinning structure. Such a pinning structure is characterized by a distance between pinning centers that is only slightly larger than  $\xi$ ; i.e., the pinning matrix is expected to have weaker interaction with vortices. Using this model, the observed elimination of both maximums in  $F_p(B)$  due to the HPA process (see Fig. 6) can be explained in a similar way. By introducing additional oxygen into the CuO chains, the HPA creates additional pinning centers, and, in this manner, makes the pinning structure more uniform. This explanation is supported by an observation of increase in  $j_c$  at lower temperatures (e.g. at 50 K, see Fig. 5) where  $\xi(T)$  decreases and the pinning structure becomes more granular. With decreasing temperature, an increase of the volume

pinning force is expected to shift the maximum of  $F_p(B)$ , observed for the NPA sample, to higher fields. This shift is clearly visible for the  $x = 0.02$  sample (see Fig. 7b). In addition, the second maximum in  $F_p(B)$ , that is absent for the  $x = 0$  sample, seems to shift above 7 T at 70 K. The drastic drop of the pinning force at these fields and temperature for the  $x = 0$  sample points again to a large difference in pinning properties between the  $x = 0$  and 0.02 samples.

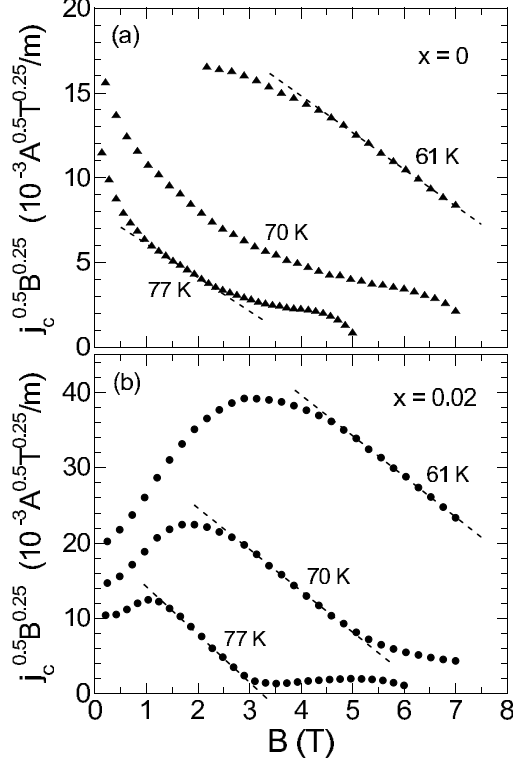


FIG. 10: Kramer's plots at 61, 70, and 77 K for the  $\text{YBa}_2\text{Cu}_{3-x}\text{Mo}_x\text{O}_{7+d}$  samples with  $x = 0$  (a) and 0.02 (b) annealed in oxygen at normal pressure. Scaling field,  $B_k(T)$ , is obtained at individual temperature as a field determined by linear extrapolation of the broken line to  $j_c = 0$ .

When thermal activation effects are negligible, the volume pinning force is usually described by the following formula:<sup>35,36</sup>  $F_p(b, T) = F_{p0}(T)b^p(1 - b)^q$ , where  $F_{p0}(T)$  is the field-independent pinning force in the absence of thermal activation and  $b = B/B^*(T)$  is a reduced field, where  $B^*(T)$  is the scaling field, and  $p$  and  $q$  depend on the relevant pinning mechanism. In this model it is usually difficult to attribute the involved coefficients to the particular pinning mechanism, because additional requirements concerning, for example, the sample geometry and grain orientation have to be fulfilled. In the Kramer's model of pinning, a simplified scaling law is used with  $f(b) = b^{1/2}(1 - b)^2$ , where  $f = F_p(b, T)/F_{p,max}(T)$ , and  $F_{p,max}(T)$  is a maximum volume pinning force for  $F_p(B)$  at each temperature.<sup>37</sup> Using Kramer's approach,  $B_{c2}(T)$  is originally taken as the scaling field  $B^*(T)$ . However, other fields related to

$B_{irr}$  rather than  $B_{c2}$  have frequently been used to model the scaling law.<sup>2,38,39,40</sup> Figure 10 shows scaled  $j_c^{1/2}B^{1/4}$  versus  $B$  (the so-called Kramer's plots), adopted to obtain the scaling field  $B_k(T) = B(T, j_c=0)$  by extrapolating  $j_c(B)$  to zero current.<sup>40,41</sup> Because  $B_k$  obtained this way is a lower limit of the measured  $B_{irr}$ , it describes properties related to the global critical current that flows through the entire sample (grain) rather than the maximal critical current preserved in some local areas. One advantage of using  $B_k$  is that it can be derived at fields much higher than those used in actual measurements. In our case, it was possible to determine  $B_k$  for temperatures down to 61 K; i.e., the temperatures where  $B_{irr}$  is too large to be measured directly.

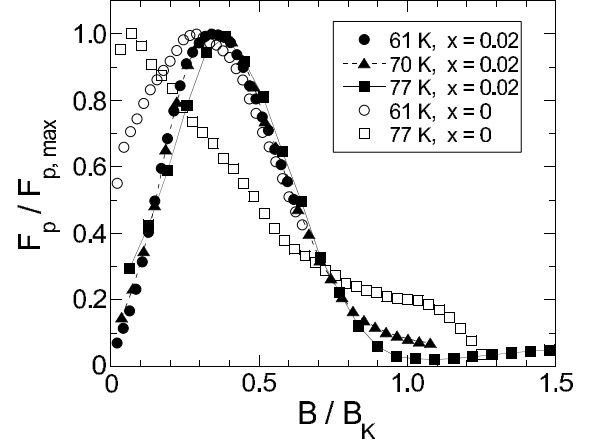


FIG. 11: Reduced pinning force,  $F_p/F_{p,max}$ , versus reduced magnetic field,  $B/B_k$ , for the non-substituted ( $x = 0$ , open symbols) and Mo-substituted ( $x = 0.02$ , closed symbols)  $\text{YBa}_2\text{Cu}_{3-x}\text{Mo}_x\text{O}_{7+d}$  samples at 61 (circles), 70 (triangles), and 77 K (squares). For the definition of  $F_{p,max}$  and  $B_k$  see text.

The scaling behavior of the volume pinning force is shown above 60 K in Fig. 11 for the  $x = 0$  and 0.02 samples. The scaling is not expected to hold at lower temperatures where additional pinning by regions between the  $\text{CuO}_2$  double planes dominates. The scaled curves in the temperature range from 61 to 77 K collapse to a single curve for  $x = 0.02$ , proving that a single pinning mechanism is responsible for increase of the critical currents. This excellent scaling of  $F_p(B)$  indicates that the  $\text{Mo}_2\text{O}_{11}$  dimers, the main defects introduced by substitution, create pinning centers that are dominant at these temperatures. The flux creep that intensifies at higher temperatures may cause a small deviation from the scaling law, as observed at 77 K. Generally, such thermally assisted flux motion leads to a breakdown of the scaling behavior because no clear separation between effects of the field and temperature is possible.<sup>42</sup> At elevated temperatures, the thermally assisted flux flow results frequently in a tail at the highest fields, exactly what is observed for the  $x = 0.02$  sample at 77 K. For  $x = 0$ , no universal scaling is observed, indicating that several different pinning

mechanisms may be dominant, depending on fields and temperatures.

## VI. SUMMARY AND CONCLUSION

We have shown that, by synthesizing  $\text{YBa}_2\text{Cu}_{3-x}\text{Mo}_x\text{O}_{7+d}$  materials in an oxygen atmosphere, it is possible to drive the substituted Mo ions into the chain region of the crystal structure. The Mo ions appear to form extended defects, most likely the  $\text{Mo}_2\text{O}_{11}$  dimers formed from nearest neighbor  $\text{MoO}_6$  octahedra. High-pressure oxygen annealing restores  $T_c \approx 92$  K. By studying the field and temperature dependence of the intragrain critical currents, we have shown that the Mo substitution introduces an important contribution to the irreversibility magnetization in agreement with our previous studies on the tetragonal  $\text{YBaSrCu}_{3-x}\text{Mo}_x\text{O}_{7+d}$  superconductor with  $T_c \approx 86$  K.<sup>3</sup> The large enhancement of the intragrain critical current density has been found for  $\text{YBa}_2\text{Cu}_{3-x}\text{Mo}_x\text{O}_{7+d}$  at elevated fields and temperatures as a distinct peak effect observed in  $j_c(B)$  for compositions with a small Mo-substitution level  $x = 0.02$ . Based on magnetization data, we infer that the  $\text{Mo}_2\text{O}_{11}$  dimers introduce additional pinning that is dominant at temperatures above 30 K by locally perturbing superconductivity in the  $\text{CuO}_2$  planes. We have shown that for the Mo-substituted samples, the pinning force scales with a characteristic field  $B_k$  which is related to the irreversibility field rather than to the upper critical field. The excellent scaling behaviour that

is observed over a wide field and temperature range for the Mo-substituted samples provides additional support for the substitution-induced pinning centers.

For the composition with  $x = 0.02$ , the intragrain critical current density has been increased by a factor of 3 to 4 at temperatures around 50 K and fields of about 6 T. An additional improvement of the critical current density could be expected at lower fields if ordering of the  $\text{Mo}_2\text{O}_{11}$  dimers is achieved along the  $c$ -axis. The annealing at high oxygen pressure, which introduces additional oxygen into the structure, reduces the irreversibility of the  $M(B)$  loops and shifts the maximum of the fishtail effect to much higher fields. This suggests that HPA creates a new type of pinning centers that are effective at higher vortex densities. Thus, for the optimized  $\text{YBa}_2\text{Cu}_{3-x}\text{Mo}_x\text{O}_{7+d}$ , the best intragrain critical currents should be obtained for material with  $x = 0.01 - 0.02$  and optimized oxygen content prepared under controlled oxygen pressure. Additional improvements of  $j_c$  are possible for the  $\text{YBa}_{2-y}\text{Sr}_y\text{Cu}_{3-x}\text{Mo}_x\text{O}_{7+d}$  materials when combined effects of the Mo- and Sr- substitutions and optimized oxygen content are utilized.

### Acknowledgments

Work at ILT&SR was supported by the Polish State Committee for Scientific Research (KBN) under Project No. 3 T10A 001 26. Work at NIU was supported by the NSF-DMR-0302617. IPNS at Argonne National Laboratory is supported by the U.S. Department of Energy, BES-MS, under Contract No. W-31-109-ENG-38.

- 
- <sup>1</sup> Ch. Jooss, R. Warthmann, H. Kronmüller, T. Haage, H.-U. Habermeier, and J. Zegenhagen, *Phys. Rev. Lett.* **82**, 632 (1999), and some references therein.
  - <sup>2</sup> B. Martinez, X. Obradors, A. Gou, V. Gomis, S. Piñol, J. Fontcuberta, and H. Van Tol, *Phys. Rev. B* **53**, 2797 (1996).
  - <sup>3</sup> K. Rogacki, B. Dabrowski, O. Chmaissem, and J. D. Jorgensen, *Phys. Rev. B* **63**, 054501 (2000).
  - <sup>4</sup> T. Haugan, P. N. Barnes, R. Wheeler, F. Meisenkothen, and M. Sumption, *Nature* **430**, 867 (2004).
  - <sup>5</sup> J. L. MacManus-Driscoll, S. R. Foltyn, Q. X. Jia, H. Wang, A. Serquis, L. Civale, B. Maiorov, M. E. Hawley, M. P. Maley, and D. E. Peterson, *Nature Mater.* **3**, 439 (2004).
  - <sup>6</sup> L. Shlyk, G. Krabbes, G. Fuchs, and K. Nenkov, *Appl. Phys. Lett.* **86**, 092503 (2005).
  - <sup>7</sup> Y. Zhao, C. H. Cheng, and J. S. Wang, *Supercond. Sci. Technol.* **18**, S43 (2005).
  - <sup>8</sup> A. Snezhko, T. Prozorov, and R. Prozorov, *Phys. Rev. B* **71**, 024527 (2005).
  - <sup>9</sup> L. Civale, *Supercond. Sci. Technol.* **10**, A11 (1997).
  - <sup>10</sup> D. Niebieskikwiat, A. Silhanek, L. Civale, G. Nieva, P. Levy, and L. Krusin-Elbaum, *Phys. Rev. B* **63**, 144504 (2001).
  - <sup>11</sup> J. R. Thompson, J. G. Ossandon, L. Krusin-Elbaum, H. J. Kim, K. J. Song, D. K. Christen, and J. L. Ullmann, *Physica C* **378 – 381**, 409 (2002).
  - <sup>12</sup> See *Introduction* in Ref. 3 and references cited therein.
  - <sup>13</sup> J. M. Tarascon, P. Barboux, P. F. Miceli, L. H. Greene, G. W. Hull, M. Eibschutz, and S. A. Sunshine, *Phys. Rev. B* **37**, 7458 (1988).
  - <sup>14</sup> B. W. Veal, W. K. Kwok, A. Umezawa, G. W. Crabtree, J. D. Jorgensen, J. W. Downey, L. J. Nowicki, A. W. Mitchell, A. P. Paulikas, and C. H. Sowers, *Appl. Phys. Lett.* **51**, 279 (1989).
  - <sup>15</sup> C. T. Lin, A. M. Niraimathi, Y. Yan, K. Peters, H. Bender, E. Schönherr, and E. Gmelin, *Physica C* **272**, 285 (1996).
  - <sup>16</sup> D. G. Kuberkar, J. A. Bhalodia, G. J. Balधा, I. A. Shaikhutpal Joshi, and R. G. Kulkarni, *Appl. Supercond.* **3**, 357 (1995).
  - <sup>17</sup> P. Li, J. Zhang, G. Cao, C. Jing, and S. Cao, *Phys. Rev. B* **69**, 224517 (2004).
  - <sup>18</sup> A. C. Larson and R. B. von Dreele, "General Structure Analysis System (GSAS)", Los Alamos National Laboratory Report LAUR 86-748 (2000); B. H. Toby, EXPGUI, a graphical user interface for GSAS, *J. Appl. Cryst.* **34**, 210 (2001).
  - <sup>19</sup> B. Dabrowski, K. Rogacki, J. W. Koenitzer, K. R. Poeppelmeier, and J. D. Jorgensen, *Physica C* **277**, 24 (1997).
  - <sup>20</sup> D.-X. Chen, A. Sanchez, T. Puig, L. M. Martinez, and J. S. Munoz, *Physica C* **168**, 652 (1990).

- <sup>21</sup> A. M. Campbell, F. J. Blunt, J. D. Johnson, and P. A. Freeman, *Cryogenics* **31**, 732 (1991).
- <sup>22</sup> L. Balents and M. Kardar, *Phys. Rev. B* **49**, 13030 (1994).
- <sup>23</sup> L. Civale, M. W. McElfresh, A. D. Marwick, F. Holtzberg, C. Feild, J. R. Thompson, and D. K. Christen, *Phys. Rev. B* **43**, R13732 (1991).
- <sup>24</sup> G. Ravi Kumar, and P. Chaddah, *Phys. Rev. B* **39**, 4704 (1989).
- <sup>25</sup> Th. Wolf, A.-C. Bornarel, H. Küpfer, R. Meier-Hirmer, and B. Obst, *Phys. Rev. B* **56**, 6308 (1997).
- <sup>26</sup> M. Murakami, S. Gotoh, H. Fujimoto, K. Yamaguchi, N. Koshizuka, and S. Tanaka, *Supercond. Sci. Technol.* **4**, S43 (1991).
- <sup>27</sup> M. Murakami, K. Yamaguchi, H. Fujimoto, N. Nakamura, T. Taguchi, N. Koshizuka, and S. Tanaka, *Cryogenics* **32**, 930 (1992).
- <sup>28</sup> H. Küpfer, A. A. Zhukov, A. Will, W. Jahn, R. Meier-Hirmer, Th. Wolf, V. I. Voronkova, M. Kläser, and K. Saito, *Phys. Rev. B* **54**, 644 (1996).
- <sup>29</sup> D. R. Nelson, and V. M. Vinokur, *Phys. Rev. Lett.* **68**, 2398 (1992).
- <sup>30</sup> D. R. Nelson, and V. M. Vinokur, *Phys. Rev. B* **48**, 13060 (1993).
- <sup>31</sup> V. V. Moshchalkov, V. V. Metlushko, G. Güntherodt, I. N. Goncharov, A. Yu. Didyk, and Y. Bruynseraede, *Phys. Rev. B* **50**, R639 (1994).
- <sup>32</sup> O. Chmaissem, D. N. Argyriou, D. G. Hinks, J. D. Jorgensen, B. G. Storey, H. Zhang, L. D. Marks, Y. Y. Wang, V. P. Dravid, and B. Dabrowski, *Phys. Rev. B* **52**, 15636 (1995).
- <sup>33</sup> J. D. Jorgensen, D. G. Hinks, O. Chmaissem, D. N. Argyriou, J. F. Mitchell, and B. Dabrowski, in *Proceedings of the 1st Polish-US Conference on High Temperature Superconductivity*, Wroclaw and Duszyniki Zdrój, Poland, 1995, *Lecture Notes in Physics* Vol. 475, edited by J. Klamut et al. (Springer-Verlag, Berlin, 1996), pp. 1-15.
- <sup>34</sup> A. I. Larkin, and Yu. N. Ovchinnikov, *J. Low Temp. Phys.* **34**, 409 (1979).
- <sup>35</sup> A. M. Campbell, and J. E. Evetts, *Adv. Phys.* **21**, 199 (1972).
- <sup>36</sup> D. Dew-Hughes, *Philos. Mag.* **30**, 293 (1974).
- <sup>37</sup> E. J. Kramer, *J. Appl. Phys.* **44**, 1360 (1973).
- <sup>38</sup> A. Umezawa, W. Zhang, A. Gurevich, Y. Feng, E. E. Hellstrom, and D. C. Larbalestier, *Nature* **364**, 129 (1993).
- <sup>39</sup> T. Higuchi, S. I. Yoo, and M. Murakami, *Phys. Rev. B* **59**, 1514 (1999).
- <sup>40</sup> D. C. Larbalestier et al., *Nature* **410**, 186 (2001).
- <sup>41</sup> D. Dew-Hughes, *Philos. Mag.* **55**, 459 (1987).
- <sup>42</sup> L. Niel, *Cryogenics*, **32**, 975 (1992).